Compressive sensing beamforming based on covariance for acoustic imaging with noisy measurements

Siyang Zhong and Qingkai Wei
Department of Mechanics and Aerospace, College of Engineering, Peking University, Beijing, 100871, China
zhongsy@pku.edu.cn, weiqingkai@pku.edu.cn

Xun Huang[a)]
State Key Laboratory of Turbulence and Complex Systems, Department of Aeronautics and Astronautics, College of Engineering, Peking University, Beijing, 100871, China
huangxun@pku.edu.cn

Abstract: Compressive sensing, a newly emerging method from information technology, is applied to array beamforming and associated acoustic applications. A compressive sensing beamforming method (CSB-II) is developed based on sampling covariance matrix, assuming spatially sparse and incoherent signals, and then examined using both simulations and aeroacoustic measurements. The simulation results clearly show that the proposed CSB-II method is robust to sensing noise. In addition, aeroacoustic tests of a landing gear model demonstrate the good performance in terms of resolution and sidelobe rejection.

PACS numbers: 43.60.Fg [CG]
Date Received: July 10, 2013 **Date Accepted:** September 25, 2013

1. Introduction

Compressive sensing,[1–5] a new signal processing strategy from the field of information technology, reduces sampling efforts extensively by conducting L_1 optimization. This paper will apply this idea to beamforming techniques[6] that visualize signal of interest as measured by a sensor array. Potential applications can be found in acoustics.[7–12]

Recently, some compressive sensing based beamforming methods have been developed for direction-of-arrival estimation problem.[13,14] The first paper demonstrated in numerical simulations that only a few samples are required compared with conventional beamforming. Compressive sensing beamforming was also applied to undersea data, manipulating the sensing matrix to maintain a stable calculation.[14] Most works in the literature use uniformly linear array[13–16] and are examined only by simulation data. Aeroacoustic testing, on the other hand, uses a different array layout. Aeroacoustic experiments performed in wind tunnel and anechoic chamber jet facility usually contain strong background noise at broadband frequencies. These issues from the specific application impose challenges to compressive sensing based beamforming.

This article will present a novel compressive sensing beamforming method and apply it to an aeroacoustic problem. It was verified using both simulated data with various signal-to-noise ratios (SNR) and measured aeroacoustic test data.

[a)]Author to whom correspondence should be addressed.

2. Preliminary knowledge

2.1 Wave model

Beamforming is generally conducted in the frequency domain. For a single signal of interest $S(j\omega) \in \mathfrak{C}^1$ in a free propagation space, using the associated Green's function, we have

$$\mathbf{Y}(j\omega) = \frac{1}{4\pi \mathbf{r}} S(j\omega) e^{-j\omega\tau} = \mathbf{G}_v(\mathbf{r}, j\omega) S(j\omega), \tag{1}$$

where $\mathbf{Y} \in \mathfrak{C}^{M\times 1}$ are measurements of the array sensors; $\mathbf{r} \in \Re^{M\times 1}$ are the distances between S and sensors; $j = \sqrt{-1}$; $\boldsymbol{G}_v \in \mathfrak{C}^{M\times 1}$ is the associated steering vector; and ω is angular frequency. $(j\omega)$ and $(\mathbf{r}, j\omega)$ are usually omitted for brevity. The subscript $(\cdot)_v$ suggests that $\mathbf{G}_v$ is a vector.

The situation becomes complicated for multiple signals of interest plus measurement noise. For clarity, the array output is represented in the scalar form

$$\begin{bmatrix} Y_1 \\ \vdots \\ Y_i \\ \vdots \\ Y_M \end{bmatrix} = \begin{bmatrix} G_{11} & \cdots & G_{1k} & \cdots & G_{1N} \\ & & \vdots & & \\ G_{i1} & \cdots & G_{ik} & \cdots & G_{iN} \\ & & \vdots & & \\ G_{M1} & \cdots & G_{Mk} & \cdots & G_{MN} \end{bmatrix} \begin{bmatrix} S_1 \\ \vdots \\ S_k \\ \vdots \\ S_N \end{bmatrix} + \begin{bmatrix} N_1 \\ \vdots \\ N_i \\ \vdots \\ N_M \end{bmatrix}, \tag{2}$$

where $Y_i(j\omega)$ is the ith sensory measurements; G_{ik} is the steering vector between the ith sensor and the kth signal of interest; $S_k(j\omega)$ is the kth signal of interest; and $N_i(j\omega)$ is the collective measurement noise of the ith sensor. Potential noise sources include external background interference and inherent electronic noise during data acquisition. Equation (2) can be written as

$$\mathbf{Y} = \mathbf{GS} + \mathbf{N}, \tag{3}$$

where $\mathbf{G} \in \Re^{M\times N}$ is the associated matrix of steering vectors; and $\mathbf{S} \in \mathfrak{C}^{N\times 1}$ and $\mathbf{N} \in \mathfrak{C}^{M\times 1}$. Generally, it is assumed that $\mathbf{S}$ and $\mathbf{N}$ are zero-mean and statistically independent. In this work, the SNR of the kth sensor is defined in decibels,

$$\mathrm{SNR}_{\mathrm{dB}} = 10\log_{10}\left(\frac{\left|\sum_{i=1}^{N} G_{ki}S_i\right|^2}{|N_i|^2}\right). \tag{4}$$

2.2 Compressive sensing

Candes *et al.*[1] proposed that a perfect reconstruction of a discrete-time signal $\sigma \in \mathcal{C}^N$ using sub-Shannon sampling rates is possible, as long as σ is sparse in some Hilbert basis $\Psi \in \mathcal{C}^{N\times N}$, that is, $\sigma = \Psi\alpha$, $\alpha \in \mathcal{C}^N$. The so-called *sparsity* means that the number of nonzero entries in α is pretty small, i.e., $\|\alpha\|_0 \ll N$.

According to compressive sensing theory, we can perform a small number of measurements to collect $\mathbf{y} = \Phi\sigma$, where $\mathbf{y} \in \mathcal{C}^K$ and the sensing matrix $\Phi \in \mathcal{C}^{K\times N}$, in the form of underdetermined linear equations. The sparse signal can then be reconstructed from those K projections by solving an L_1 regularization optimization[1]

$$\arg\min \|\hat{\alpha}\|_1, \text{ subject to } \Phi\Psi\hat{\alpha} = y_i, i = 1, ..., K, \tag{5}$$

where $\hat{(\cdot)}$ represents the recovered estimation.

For those measurements contaminated by noise, the programming with an error constraint should be adopted as the following:[3]

$$\arg\min \|\hat{\alpha}\|_1, \text{ subject to } \|y - \Phi\Psi\hat{\alpha}\|_2 \leqslant \delta, \delta > 0. \tag{6}$$

Generally, δ is empirically chosen according to given SNR. The above programming can be solved using available convex optimization tools, such as CVX.[17] Once $\hat{\alpha}$ is achieved, the original signal σ can be recovered as $\Psi\hat{\alpha}$.

3. Compressive sensing beamforming

In this work, signals of interest are presumably regarded as spatially sparse. The same assumption has been adopted in the literature[18] for bearing estimation. Then, by comparing with Eq. (6) and Eq. (3), a narrowband compressive sensing beamforming can be simply performed as the following:[15]

$$\arg\min \|\hat{\mathbf{S}}\|_1, \text{ subject to } \|\mathbf{Y} - \mathbf{G}\hat{\mathbf{S}}\|_2 \leqslant \delta\,,\ \delta \geqslant 0, \tag{7}$$

where $\delta = 0$ if measurements are free of noise (i.e., SNR $= \infty$). For convenience, this compressive sensing beamforming method is denoted by CSB-I in the following. It will be shown in Sec. 4 that CSB-I fails for measurements of poor SNR.

To improve robust performance, we developed a novel compressive sensing beamforming method, which is called CSB-II throughout this paper, based on so-called cross spectrum matrix (also known as covariance matrix or cross-spectral density matrix), which is defined by

$$\mathbf{R} = \mathrm{E}\{\mathbf{YY}^*\} = \begin{bmatrix} \mathrm{E}\{Y_1 Y_1^*\} & \mathrm{E}\{Y_1 Y_2^*\} & \cdots & \mathrm{E}\{Y_1 Y_M^*\} \\ \mathrm{E}\{Y_2 Y_1^*\} & \mathrm{E}\{Y_2 Y_2^*\} & \cdots & \mathrm{E}\{Y_1 Y_M^*\} \\ & & \vdots & \\ \mathrm{E}\{Y_M Y_1^*\} & \mathrm{E}\{Y_M Y_2^*\} & \cdots & \mathrm{E}\{Y_M Y_M^*\} \end{bmatrix}, \tag{8}$$

where $\mathbf{R} \in \Re^{M\times M}$, $\mathrm{E}\{\cdot\}$ represents expectations, and the symbol $(\cdot)^*$ denotes the conjugate transpose.

Assuming a reshape where each row of $\mathbf{R}$ is stacked behind the previous ones, we have

$$\mathbf{R}_V = (\mathrm{E}\{Y_1 Y_1^*\}, \mathrm{E}\{Y_1 Y_2^*\}, \ldots, \mathrm{E}\{Y_1 Y_M^*\}, \ldots, \mathrm{E}\{Y_M Y_1^*\}, \ldots, \mathrm{E}\{Y_M Y_M^*\})^T. \tag{9}$$

It should be noticed that $\mathbf{R}_V$ is a very long vector $\in \mathfrak{C}^{M^2\times 1}$.

From Eq. (3), we have

$$\mathrm{E}\{\mathbf{YY}^*\} = \mathrm{E}\{\mathbf{GSS}^*\mathbf{G}_{m_I}^*\} + \mathrm{E}\{\mathbf{NN}^*\}, \tag{10}$$

where the relation of $\mathrm{E}\{\mathbf{SN}^*\} = 0$ is assumed. Physically, it suggests that background noise and signals of interest are incoherent. Furthermore, assuming $\mathrm{E}\{S_i S_j^*\} = 0$, $\mathrm{E}\{N_i N_j^*\} = 0$, $\forall i \neq j$, since signal sources are presumably incoherent across frequencies, we have

$$\mathbf{SS}^*\mathbf{G}_{m_I}^* = \begin{bmatrix} S_1 S_1^* & 0 & \cdots & 0 \\ 0 & S_2 S_2^* & \cdots & 0 \\ 0 & 0 & \vdots & 0 \\ 0 & 0 & \cdots & S_M S_M^* \end{bmatrix} \begin{bmatrix} G_{11}^* & \cdots & G_{M1}^* \\ \vdots & & \vdots \\ G_{1N}^* & \cdots & G_{MN}^* \end{bmatrix} = \begin{bmatrix} S_1 S_1^* G_{11}^* & \cdots & S_1 S_1^* G_{M1}^* \\ \vdots & & \vdots \\ S_N S_N^* G_{1N}^* & \cdots & S_N S_N^* G_{MN}^* \end{bmatrix} \tag{11}$$

and

$$\mathbf{GSS}^{*}\mathbf{G}_{m_I}^{*} = \begin{bmatrix} G_{11} & \cdots & G_{1N} \\ \vdots & & \vdots \\ G_{M1} & \cdots & G_{MN} \end{bmatrix} \begin{bmatrix} S_1 S_1^* G_{11}^* & \cdots & S_1 S_1^* G_{M1}^* \\ \vdots & & \vdots \\ S_N S_N^* G_{1N}^* & \cdots & S_N S_N^* G_{MN}^* \end{bmatrix}$$
$$= \begin{bmatrix} S_1 S_1^* G_{11} G_{11}^* + \cdots S_N S_N^* G_{1N} G_{1N}^*, & \ldots, & S_1 S_1^* G_{11} G_{M1}^* + \cdots S_N S_N^* G_{1N} G_{MN}^* \\ \vdots & & \vdots \\ S_1 S_1^* G_{M1} G_{11}^* + \cdots S_N S_N^* G_{MN} G_{1N}^*, & \ldots, & S_1 S_1^* G_{M1} G_{M1}^* + \cdots S_N S_N^* G_{MN} G_{MN}^* \end{bmatrix}. \tag{12}$$

Once again, reshaping each row of the above matrix, we get

$$\mathbf{R}_V = \begin{bmatrix} G_{11} G_{11}^* & G_{12} G_{12}^* & \cdots & G_{1N} G_{1N}^* \\ G_{11} G_{21}^* & G_{12} G_{22}^* & \cdots & G_{1N} G_{2N}^* \\ & & \vdots & \\ G_{M1} G_{M1}^* & G_{M2} G_{M2}^* & \cdots & G_{MN} G_{MN}^* \end{bmatrix} \begin{bmatrix} S_1 S_1^* \\ S_2 S_2^* \\ \vdots \\ S_N S_N^* \end{bmatrix} + \begin{bmatrix} N_1 N_1^* \\ N_2 N_2^* \\ \vdots \\ N_N N_N^* \end{bmatrix} = G_{II}\mathrm{P} + \mathrm{Q}, \tag{13}$$

where $\mathbf{G}_{\mathrm{II}} \in \mathfrak{C}^{M^2 \times N}$, $\mathbf{P} = [S_1 S_1^*, S_2 S_2^*, \ldots, S_N S_N^*]^T \in \Re^{N \times 1}$, and $\mathrm{Q} = [N_1 N_1^*, N_2 N_2^*, \ldots, N_M N_M^*]^T \in \Re^{M^2 \times 1}$. It is worthwhile to notice that the dimension of $\mathbf{G}_{II}$ in CSB-II is much larger than the dimension of $\mathbf{G}$ in CSB-I.

Then, we can propose the CSB-II method, which solves

$$\arg\min \|\hat{\mathbf{P}}\|_1, \text{ subject to } \hat{\mathbf{P}} > 0, \ \|\hat{\mathbf{R}}_V - G_{II}\hat{\mathbf{P}}\|_2 \leqslant \delta, \delta > 0. \tag{14}$$

We should mention that the optimization result $\hat{\mathbf{P}}$ in CSB-II is positive real-valued intensity instead of complex acoustic amplitude in CSB-I. As the dimension of $\mathbf{G}_{II}$ in Eq. (13) is much larger than that of $\mathbf{G}$ in Eq. (7), the calculation speed of the CSB-II method is lower than that of the CSB-I method.

4. Results and discussion

Test data achieved in our previous experiments[19] is used to demonstrate compressive sensing beamforming methods. The experimental setup is briefly introduced for the completeness of this paper. The experiments were conducted in an anechoic chamber facility ($9.15\,\mathrm{m} \times 9.15\,\mathrm{m} \times 7.32\,\mathrm{m}$) at ISVR, University of Southampton. Figure 1 shows the setup. A nozzle ($500\,\mathrm{mm} \times 350\,\mathrm{mm}$) connecting to a plenum chamber produces a jet flow of $U_\infty = 30\,\mathrm{m/s}$. An airframe model representing a part of a landing gear was studied in experiments. The corresponding Reynolds number based on the cylinder diameter is 2.1×10^5.

An array of 56 electret microphones (PanasonicWM-60A) is placed on the ground, underneath the test model. The coordinates shown in Fig. 1 are used throughout the rest of the paper. The distance between the array and the model is 0.7 m. The center of the array is aligned with the origin. The sensitivity of each microphone is -45 ± 5 dBV/Pa. The frequency response of each WM-60A microphone is calibrated to decrease amplitude and phase deviations from a B&K 4189 microphone. The layout of the microphones is a multi-arm spiral line, which is *de facto* adopted in acoustic tests (pp.118–128, in Ref. 20), largely different from those uniformly linear arrays usually found in compressive sensing beamforming works.[15,16]

Before working on those experimental data, we first conducted simulations that easily quantify the performance of the aforementioned methods. We assume free space propagation of a monopole tonal source locating at the origin, 1 m away from the array. The frequency of the source is 5 kHz. For this simple case, 10 microphones randomly chosen within the 56 microphone array are used to yield the beamforming results. In

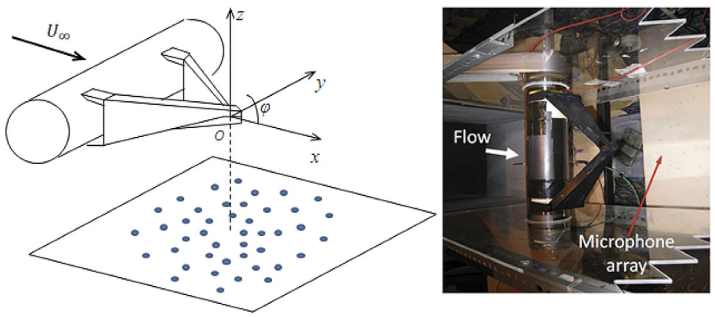

Fig. 1. (Color online) The setup of experimental units.

addition, we assume that each sensor also perceives a white noise. Various SNR levels, from ∞ to -10 dB, have been tested. According to Eq. (4), SNR $= \infty$ suggests a negligible noise; SNR $= 0$ dB suggests that the power from the monopole signal equals the power from the background noise; and SNR $= -10$ dB suggests that the power of the background noise is ten times greater than the power of the monopole signal.

Figures 2(a) and 2(b) show the normalized narrowband beamforming results using the CSB-I method. In Fig. 2(a), the simulated measurements are free of background noise (i.e., SNR $= \infty$). It can be seen that the CSB-I method perfectly capture the desired signal with very fine resolution and nice sidelobe rejection. However, as SNR decreases, we found that the CSB-I method quickly fails to output reasonable results. For example, when SNR $= -10$ dB, Fig. 2(b) shows that false signal sources scatter on the entire imaging domain. In contrast, Fig. 2(c) shows that the CSB-II

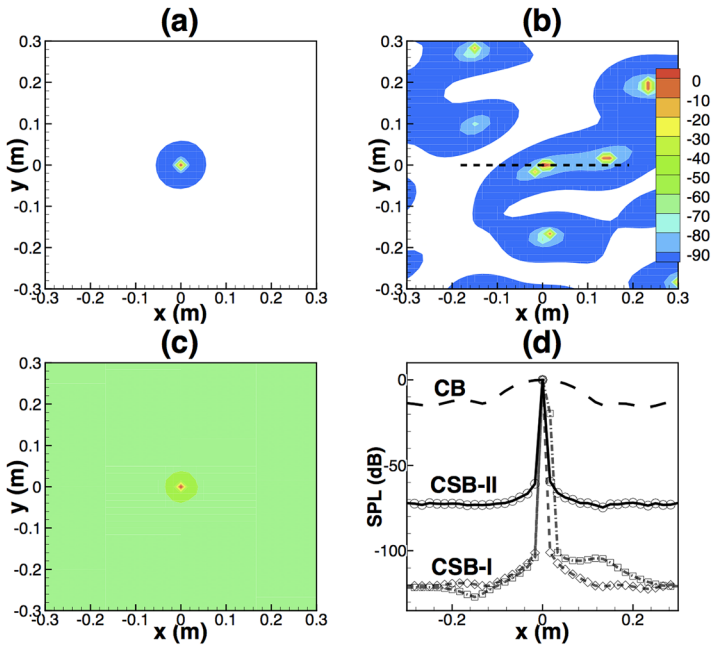

Fig. 2. (Color online) Beamforming results of the monopole case at 5 kHz, where (a) SNR $= \infty$, CSB-I; (b) SNR $= -10$ dB, CSB-I; (c) SNR $= -10$ dB, CSB-II; and (d) the x-axial only performance, (—) the CB result for SNR $= -10$ dB, (◇) the CSB-I result for SNR $= \infty$ (□) the CSB-I result for SNR $= -10$ dB, and (○) the CSB-II result for SNR $= -10$ dB. The contour levels in (a)–(c) are set between -100 and 0 dB. The levels below -100 dB are cut off.

method is still able to capture the mainlobe as well as maintain a good sidelobe rejection. The dynamic range is, however, diminished from 100 to 60 dB.

Figure 2(d) examines the x-axial performance on the dashed line [shown in Fig. 2(b)]. The conventional beamforming (CB) result is also shown in comparing with compressive sensing beamforming methods. The following expression is used in the calculation of the CB method:

$$(S\hat{S}^*) = \mathbf{W}^*\hat{\mathbf{R}}\mathbf{W},\ \mathbf{W} = (\mathrm{G}_v^*\mathrm{G}_v)^{-1}\mathrm{G}_v. \tag{15}$$

The above CB method is narrowband, only for a single gridpoint. We have to scan 1600 gridpoints of the imaging plane one by one to yield desired images at frequency ranges of interest. Figure 2(d) shows that the CB method produces a very broad mainlobe. The associated dynamic range is slightly over 10 dB.

Figure 2(d) clearly identify the distinctive performance of compressive sensing beamforming methods, in terms of resolution and dynamic range. However, the CSB-I method fails when SNR is just over 0 dB. In contrast, the CSB-II method can suppress detrimental interference of noisy measurements subject to noise of SNR $= -10$ dB. As a result, only the CSB-II method is applied to the following measurement data, which generally consists of distributions of multiple broadband noise sources and poor SNR. The bluff body model representing the main part of a landing gear is used (see Fig. 1). The number of signals of interest and the respective SNR of each sensor are unknown. Measurements from all 56 sensors are used.

The CSB-I method fails to yield meaningful results. Only the CSB-II results are compared to the results of the CB method at various frequencies. Figure 3 shows some results at 2 and 5 kHz. The contour levels are between -10 and 0 dB. Compared to the CB results, the CSB-II results have a better resolution (with narrow mainlobes) and smaller sidelobe levels. It is easy to see that the imaging quality is improved with the proposed compressive sensing based beamforming method.

5. Summary

Compressive sensing, the newly emerging method from information technology, could significantly impact acoustic research and applications. In this article, we first

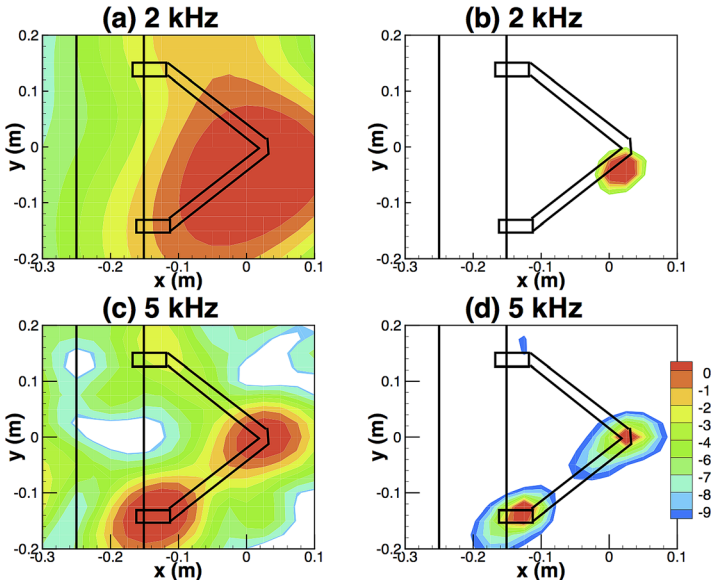

Fig. 3. (Color online) Acoustic images: (a),(b) 2 kHz; (c),(d) 5 kHz; (a),(c) using the CB algorithm and (b),(d) using the CSB-II algorithm.

introduced the fundamentals of compressive sensing theory. After that, we implemented two different compressive sensing based beamforming methods (CSB-I and CSB-II) for presumably spatially sparse and incoherent signals.

Compressive sensing beamforming methods are first examined in simulations and then using aeroacoustic experimental data. The simulation case clearly shows that the CSB-I method is sensitive to the sensing noise. The CSB-II method, on the other hand, is more robust to noisy measurements. We believe this performance has connection with the so-called restricted isometry property.[1] Detailed analysis is beyond the scope of this note.

The results suggest that the proposed CSB-II method is robust to potential interference and noise, producing acoustic images with a significant improvement of resolution. As a result, the effort of classical deconvolution post-processing in aeroacoustic can be saved using the proposed compressive sensing beamforming.

Acknowledgments

This research was supported by the NSF Grant of China (Grants Nos. 11172007 and 11322222). The experiments were conducted at ISVR, University of Southampton. We acknowledge Professor Xin Zhang for his support with the experiments.

References and links

[1]E. J. Candes, J. Romberg, and T. Tao, "Robust uncertainty principles: Exact signal reconstruction from highly incomplete frequency information," IEEE Trans. Inf. Theory **52**(2), 489–509 (2006).
[2]E. J. Candes, "Near-optimal signal recovery from random projections: universal encoding strategies?," IEEE Trans. Inf. Theory **52**(12), 5406–5425 (2006).
[3]E. J. Candes and M. B. Wakin, "An introduction to compressive sampling," IEEE Signal Process. Mag. **25**(2), 21–30 (2008).
[4]J. Romberg, "Imaging via compressive sampling," IEEE Signal Process. Mag. **25**(2), 14–20 (2008).
[5]R. G. Baraniuk, "More is less: signal processing and the data deluge," Science **331**(11), 717–719 (2011).
[6]B. D. Van Veen and K. M. Buckley, "Beamforming: A versatile approach to spatial filtering," IEEE ASSP Mag. **5**(2), 4–24 (1988).
[7]R. A. Gramann and J. W. Mocio, "Aeroacoustic measurements in wind tunnels using adaptive beamforming methods," J. Acoust. Soc. Am. **97**(6), 3694–3701 (1995).
[8]Y. T. Cho and M. J. Roan, "Adaptive near-field beamforming techniques for sound source imaging," J. Acoust. Soc. Am. **125**(2), 944–957 (2009).
[9]T. Yardibi, J. Li, P. Stoica, and L. N. Cattafesta, "Sparsity constrained deconvolution approaches for acoustic source mapping," J. Acoust. Soc. Am. **123**(5), 2631–2642 (2008).
[10]Y. Liu, A. R. Quayle, A. P. Dowling, and P. Sijtsma, "Beamforming correction for dipole measurement using two-dimensional microphone arrays," J. Acoust. Soc. Am. **124**(1), 182–191 (2008).
[11]L. Bai and X. Huang, "Observer-based beamforming algorithm for acoustic array signal processing," J. Acoust. Soc. Am. **130**(6), 3803–3811 (2011).
[12]X. Huang, L. Bai, I. Vinogradov, and E. Peers, "Adaptive beamforming for array signal processing in aeroacoustic measurements," J. Acoust. Soc. Am. **131**(3), 2152–2161 (2012).
[13]A. C. Gurbuz, J. H. McClellan, and V. Cevher, "A compressive beamforming method," in *Proceedings of the IEEE International Conference on Acoustics, Speech and Signal Processing, 2008* (2008).
[14]G. F. Edelmann and C. F. Gaumond, "Beamforming using compressive sensing," J. Acoust. Soc. Am. **130**(4), EL232–EL237 (2011).
[15]D. Malioutov, M. Cetin, and A. S. Willsky, "A sparse signal reconstruction perspective for source localization with sensor arrays," IEEE Trans. Sig. Proc. **53**(8), 3010–3022 (2005).
[16]N. Wagner, Y. C. Eldar, and Z. Friedman, "Compressed beamforming in ultrasound imaging," IEEE Trans. Sig. Proc. **60**(9), 4643–4657 (2012).
[17]S. Boyd and L. Vandenberghe, *Convex Optimization* (Cambridge University Press, New York, 2004).
[18]A. C. Gurbuz, V. Cevher, and J. H. McClellan, "Bearing estimation via spatial sparsity using compressive sensing," IEEE Trans. Aerosp. Electron. Syst. **48**(2), 1358–1369 (2012).
[19]X. Huang, X. Zhang, and Y. Li, "Broadband flow-induced sound control using plasma actuators," J. Sound Vib. **329**(13), 2477–2489 (2010).
[20]T. J. E. Mueller, *Aeroacoustic Measurements* (Springer, Germany, 2002).